

pubs.acs.org/ac Article

# Boosting the Brightness of Raman Tags Using Cyanostar Macrocycles

Ryo Nishiyama,<sup>∇</sup> Kei Furuya,<sup>∇</sup> Phillip McCann,<sup>∇</sup> Laura Kacenauskaite, Bo W. Laursen, Amar H. Flood, Kotaro Hiramatsu,\* and Keisuke Goda\*



Cite This: Anal. Chem. 2023, 95, 12835-12841



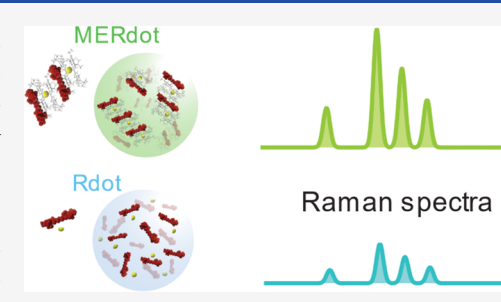
**ACCESS** I

III Metrics & More

Article Recommendations

Supporting Information

ABSTRACT: Raman probes have received growing attention for their potential use in super-multiplex biological imaging and flow cytometry applications that cannot be achieved using fluorescent probes. However, obtaining strong Raman scattering signals from small Raman probes has posed a challenge that holds back their practical implementation. Here, we present new types of Raman-active nanoparticles (Rdots) that incorporate ionophore macrocycles, known as cyanostars, to act as ion-driven and structure-directing spacers to address this problem. These macrocycle-enhanced Rdots (MERdots) exhibit sharper and higher electronic absorption peaks than Rdots. When combined with resonant broadband time-domain Raman spectroscopy, these MERdots show a ~3-fold



increase in Raman intensity compared to conventional Rdots under the same particle concentration. Additionally, the detection limit on the concentration of MERdots is improved by a factor of 2.5 compared to that of Rdots and a factor of 430 compared to that of Raman dye molecules in solution. The compact size of MERdots (26 nm in diameter) and their increased Raman signal intensity, along with the broadband capabilities of time-domain resonant Raman spectroscopy, make them promising candidates for a wide range of biological applications.

#### INTRODUCTION

Accurately characterizing the distribution and dynamics of various chemical species is of vital importance for understanding complex biological systems. To this end, chemical probes play a key role in detecting biomolecules through optical tools such as microscopy and flow cytometry. <sup>1–7</sup> By attaching antibodies coupled with chemical probes to antigens through highly selective protein—protein interactions, various biomarkers can be identified with optical tools. Fluorescence has traditionally been the gold standard for this purpose by virtue of its high brightness. <sup>8,9</sup> Recently, however, Raman probes have emerged as a promising alternative to fluorescent probes due to their high multiplex capability while maintaining excellent binding efficiency and nondestructive measurement capability. <sup>10–12</sup>

A major drawback of Raman probes is their low brightness, which significantly hinders their wider deployment in biological research. Since the cross section of Raman scattering is generally several orders of magnitude smaller than that of fluorescence, signal enhancement is necessary for making it a practical tool in biology. To overcome this hurdle, various approaches have been reported in the last decade. Metal nanoparticles for surface-enhanced Raman scattering (SERS) are popular owing to their strong Raman signal, with a potential enhancement factor of up to  $10^8$ ,  $^{14-17}$  but they are still relatively large ( $\sim$ 100 nm), which makes it difficult to reach the site of action inside of cells. Bioorthogonal Raman

probes are a promising alternative thanks to their small size, but they have a low brightness compared to other Raman probes, which limits their applicability. <sup>12,19–21</sup> Among these, Raman-active nanoparticles (Rdots<sup>22,23</sup>) are a promising approach because of their high brightness, small size, and size controllability, as well as the ease of functionalizing their surface with proteins and nucleic acids. Rdots consist of 20–60 nm polystyrene nanoparticles, in which Raman-active molecules are densely enclosed at high local concentrations of >0.25 mol/L to ensure high brightness. However, the properties of the electronic states of the tightly packed dye molecules in these particles are often significantly altered by their intermolecular interactions. <sup>24,25</sup> Due to this, it has been challenging to use Rdots under the desired electronic resonance condition.

In the present work, we demonstrate ultrabright Rdots whose Raman signals can be increased by electronic resonance with the aid of cyanostar macrocycles, which we named macrocycle-enhanced Rdots (MERdots). Specifically, we synthesized MERdots with high dye concentrations that have

Received: May 6, 2023 Accepted: July 28, 2023 Published: August 17, 2023





their intermolecular distances controlled by using cyanostar macrocycles that act as anion-binding and structure-directing spacers. The act as anion-binding and structure-directing spacers. Specifically, when 2 equiv of cyanostars are mixed with cationic cyanine dyes, they are known to form crystals that are hierarchically self-assembled into small-molecule, ionic isolation lattices (SMILES). The cyanostars bind the counter anions as a 2:1 sandwich dimer that serves as an anionic platform that stacks in a charge-by-charge array with the cationic dyes effectively isolating them from each other by  $\sim\!15$  Å. MERdots show sharper and higher electronic absorption peaks than Rdots and an  $\sim\!3$ -fold increase in Raman intensity compared to conventional Rdots under the same particle concentration. The MERdots scheme will further diversify the application range of Raman tags for biomedical research by virtue of its high multiplex ability and brightness.

## **■ EXPERIMENTAL SECTION**

The synthesis of Rdots and MERdots was performed by following the procedures described in previously published studies. 22,23,33 All procedures were conducted at room temperature. For the synthesis of Rdots, a mixture of 93.75  $\mu$ L of 26 nm polystyrene nanoparticles (4% w/v, Invitrogen, C37231), 150  $\mu$ L of F-127 (2% w/v, Invitrogen, P6867), and 356.25  $\mu$ L of deionized water was prepared in a 1.5 mL plastic tube. Subsequently, 270  $\mu$ L of tetrahydrofuran (THF) was slowly added to the tube to swell the polystyrene nanoparticles, which were then vortexed for 5 min. After vortexing, 6  $\mu$ L of an IR740-Cl solution (60 mmol/L in DMSO) was added, and the tube was vortexed for another 2 min. This process was repeated until it reached the desired dye concentration, and DMSO was added to bring the final mixture volume to 900  $\mu$ L (Table S1). The tube was vortexed for a total of 20 min. Subsequently, the mixture was transferred to a 15 mL plastic tube, and 10 mL of deionized water was slowly added to shrink the particles back down to their original size. The resulting mixture was then centrifuged at 2900g for 10 min using 100 K MWCO filters (Millipore, UFC910096) to remove the solvents. Finally, the stained nanoparticles were washed 3 times with at least 5 mL of deionized water and then suspended in deionized water.

For the synthesis of MERdots (Figure 1), the same mixture of 26 nm polystyrene nanoparticles, F-127, and deionized water was prepared in a 1.5 mL plastic tube. In contrast to the Rdot synthesis, 270  $\mu$ L of THF was initially used to dissolve the desired amount of cyanostars in a 10 mL glass vial. This

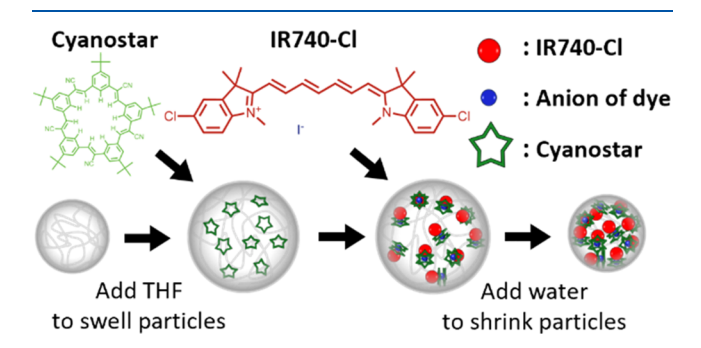


**Figure 1.** Macrocycle-enhanced Rdots (MERdots) synthesis procedure. THF containing cyanostars was added to the suspension to swell the particles and incorporate cyanostars. IR740-Cl was added to the suspension, followed by shrinking the particles by adding an excess amount of water.

solution was then slowly added to the mixture in the tube and vortexed for 15 min. Subsequently, 6  $\mu$ L of an IR740-Cl solution (30 mmol/L in DMSO) was added to the tube to achieve the desired dye concentration, and DMSO was added to bring the volume of the mixture to 900  $\mu$ L (Table S2). The mixture was then vortexed for another 10 min and transferred to a 15 mL plastic tube. Then, the MERdots were shrunk, washed, and suspended in the same manner as Rdots.

Although these MERdots can be used with various Raman spectroscopy methods, we employed Fourier transform coherent anti-Stokes Raman scattering (FT-CARS) spectroscopy as a proof of concept. This choice was motivated by the ultrafast and broadband detection capabilities of FT-CARS spectroscopy, which would be useful for fully demonstrating the potential of the synthesized MERdots for high-speed supermultiplex imaging or flow cytometry applications. The experimental setup of the rapid-scan FT-CARS spectrometer utilized in this paper is schematically shown in Figure S1. A pulse from a femtosecond Ti:sapphire laser (80 MHz pulse repetition rate, 100 nm bandwidth, 800 nm center wavelength, with 200 mW average optical power and ~20 fs pulse width) is split into a pair of pulses by a Michelson interferometer with a 12 kHz rapid-scanning resonant scanner in one of the arms and quarter-wave plates in both arms. At the output of the interferometer, the two pulses are orthogonally polarized and temporally separated with a time delay ranging from 0 to 3 ps. Both pulses first pass through a pair of chirped mirrors to compensate for dispersion and then go through a 750 nm longpass filter and are then focused onto the microfluidic channel with an objective (LCPLN, 0.65 N.A., Olympus). The first pulse (i.e., pump pulse) excites molecular vibrations whose periods are longer than the pulse width, followed by an interrogation of the molecular vibrations by the second pulse (i.e., probe pulse). When the probe pulse interacts with the vibrating molecule, it gains or loses energy depending on the phase of the vibration, resulting in the intensity change of the anti-Stokes-shifted light intensity. The anti-Stokes-shifted light is collected in the forward direction and detected by an avalanche photodiode as a function of the pump-probe delay at a rate of 24,000 spectra/s. The acquired interferograms are then digitally Fourier-transformed to obtain the Raman spectra of the sample. We averaged 10 spectra at a time to obtain better spectral quality, resulting in an effective spectral acquisition rate of 2400 spectra/s (417 µs for one spectral acquisition) in this paper.

# ■ RESULTS AND DISCUSSION

To characterize the change of the physical properties of the Rdots induced by the incorporation of cyanostars, three measurements were performed. First, as shown in Figure 2a, the ultraviolet-visible (UV-vis) absorption spectrum of the 26 nm IR740-Cl MERdots prepared with 2 molar equiv of cyanostars to dyes was recorded along with the absorption spectra of a methanol solution of IR740-Cl and conventional IR740-Cl-Rdots at various local dye concentrations but with the same average dye concentration. Here, the local dye concentration is defined by the number of dye molecules divided by the volume of the Rdots or MERdots while the average concentration is defined by the number of dye molecules divided by the total volume of the solution. Compared to the absorption spectrum of the IR740-Cl solution, high local dye concentration in the Rdots and MERdots causes a red shift of the absorption spectra from 746

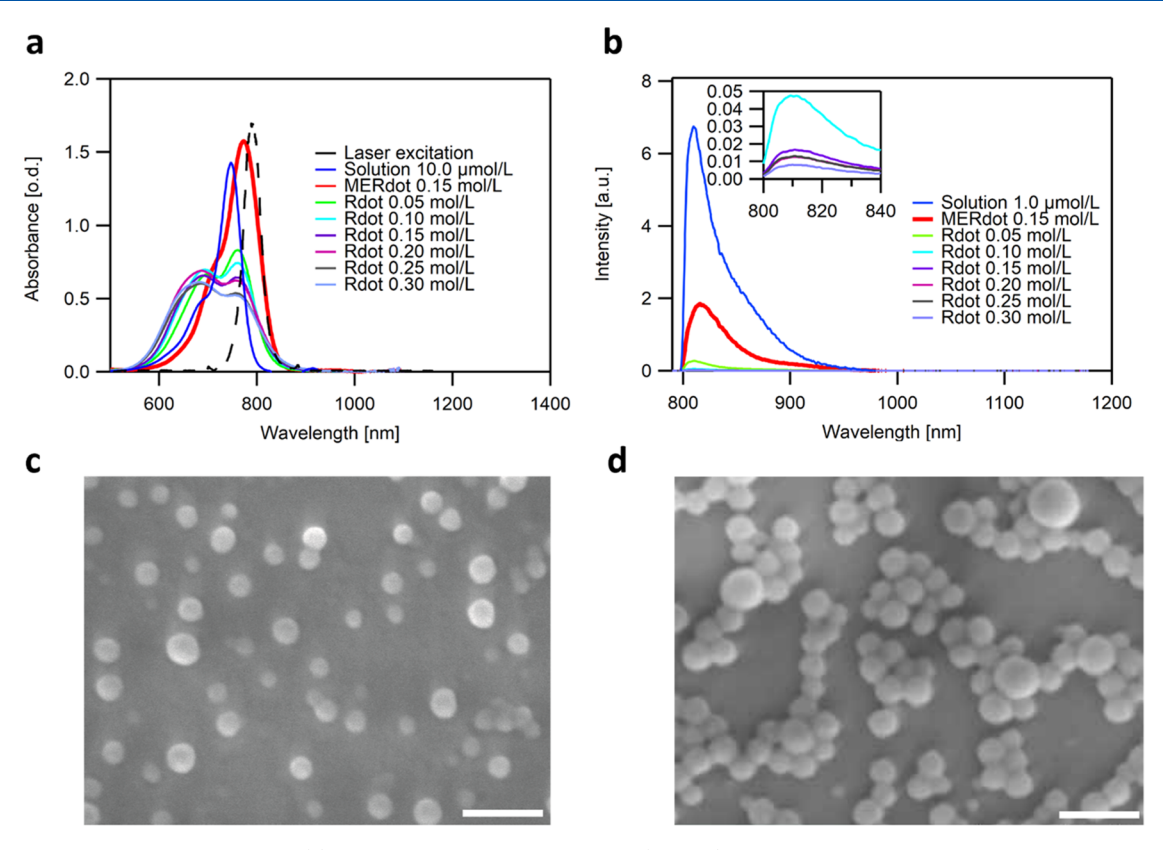
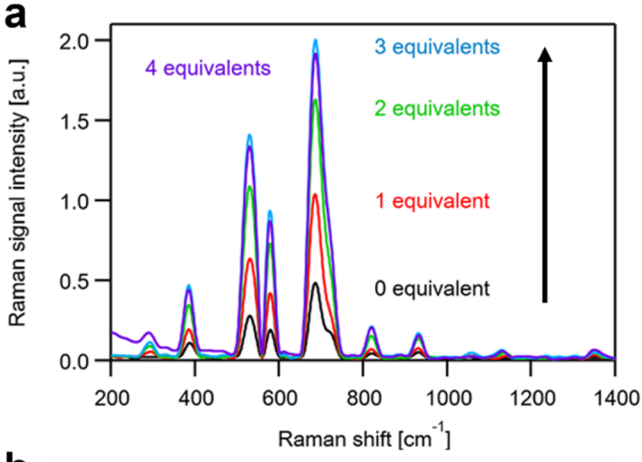
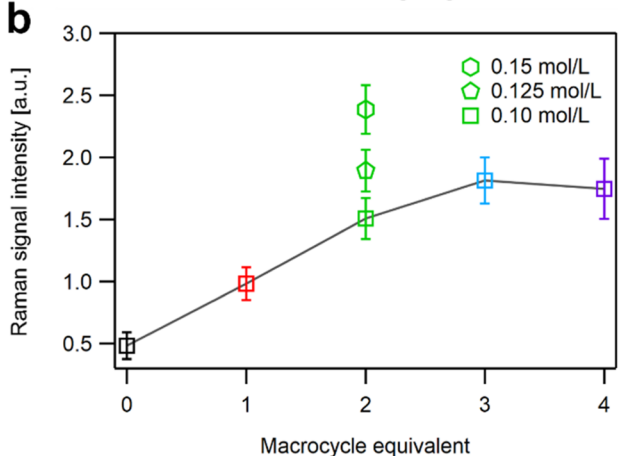


Figure 2. Characterization of MERdots. (a) Absorption spectra of Ir740-Cl (10  $\mu$ M) in a solution, conventional Rdots at different local dye concentrations, and MERdots. (b) Emission spectra of the Ir740-Cl (1  $\mu$ M) in a solution, conventional Rdots at different local dye concentrations, and macrocycle-enhanced Rdots. For both measurements, all of the samples were prepared to have the same average dye concentration. (c, d) SEM images of (c) Rdots and (d) MERdots. Scale bar: 100 nm.

to 760 nm and the absorbance of the highest peak to decrease in the case of Rdots. For the conventional Rdots, the increase of the local dye concentration leads to the distortion of the absorption spectra and a decrease of the absorbance maximum, presumably due to the formation of molecular aggregates. This change of absorption is nonideal for resonance Raman measurements, where the scattering efficiency is enhanced when the absorbance at the excitation laser wavelength is high. Making Rdots with ideal resonance enhancement has been challenging due to this effect. 33,34 For MERdots, however, the addition of cyanostars helps prevent molecular aggregation, 27-32 resulting in a large increase in the absorbance maximum and a suppression of spectral broadening. Second, the emission spectra of diluted samples from Figure 2a were recorded using an excitation wavelength of 785 nm while the emission was measured in the range of 800-1200 nm. As shown in Figure 2b, the strongest fluorescence emission comes from the IR740-Cl solution in methanol. For conventional Rdots, only extremely weak fluorescence can be detected at all local dye concentrations due to aggregation of the dye molecules in the beads. In the MERdots case, due to the addition of cyanostars as a structure-directing unit, <sup>27,28,30,35</sup> aggregation is reduced, and the fluorescence emission is partially recovered. Finally, to ensure that the incorporation of cyanostars in the Rdots does not alter the shape of the 26 nm polystyrene beads, we took scanning electron microscope (SEM) images of Rdots with a local dye concentration of 0.30 mol/L and MERdots with a local dye concentration of 0.15 mol/L prepared with 2 molar equiv of cyanostars to dyes, as can be observed in Figure 2c,d, respectively. Due to the

To explore the impact of incorporating cyanostars on the Raman signal intensity, we synthesized MERdots with a local dye concentration of 0.10 mol/L and 1 to 4 molar equiv of cyanostars to dyes. Since we know from a previous study<sup>26</sup> that the cationic cyanine dye brings the iodide counterion that binds inside a  $\pi$ -stacked dimer of the cyanostar, the ideal number of molar equivalents of cyanostar to dyes is 2. However, it has been our experience with polymers and other noncrystalline materials that 2.5–3.0 molar equiv of cyanostars to dyes often provide superior optical performance. 27,28,30,35 The FT-CARS spectra of the synthesized MERdots are shown in Figure 3a. The results indicate that the addition of cyanostars significantly increases the FT-CARS signal intensity while preserving the spectral shape. As depicted in Figure 3b, the addition of 1 equiv of cyanostars to dyes roughly doubled the Raman signal intensity, and the addition of 2 equiv tripled it. The signal intensity growth slowed down at 3 equiv, with an increase of 3.8, which can be attributed to the small difference between 2 and 3 equiv in absorbance measurements (Figure S2). At 4 equiv, the signal intensity was similar to that at 3 equiv, which may result from exceeding the uptake potential of cyanostars and dyes into the Rdots based on saturation of the charge-by-charge assembly when the 2:1 stoichiometric ratio is far surpassed. To determine the optimal conditions to





**Figure 3.** Increase of the Raman signal intensity of Rdots by cyanostars in FT-CARS spectroscopy. (a) Averaged FT-CARS spectra of MERdots synthesized with various macrocycle-dye equivalents with local dye concentrations of 0.10 mol/L (240 spectra). (b) FT-CARS peak intensities of MERdots synthesized with various macrocycle-dye equivalents. The local dye concentration in all of the samples was kept at 0.10 mol/L, except for MERdots with 2 equiv of cyanostars to dyes, where we measured local dye concentrations ranging from 0.1 to 0.15 mol/L. The error bars indicate the standard deviations of the measured FT-CARS intensities (240 spectra).

synthesize the brightest MERdots, we tested MERdots with higher local dye concentrations (0.125 and 0.15 mol/L) and 2–3 equiv of cyanostars to dyes. For MERdots with 3 equiv of cyanostars to dyes, we observed unincorporated materials even at 0.125 mol/L, as evidenced by SEM imaging (Figure S3). This infers that we have surpassed the maximum molecule uptake potential of the nanoparticles. For MERdots with 2 equiv of cyanostars to dyes, there were no unincorporated materials even at a 0.15 mol/L local dye concentration, as shown in Figure 2d, and they exhibited the highest Raman signal intensity among all of the MERdots we successfully synthesized (Figure 3b).

Next, we measured the Raman signal intensity of Rdots and MERdots at various particle concentrations (as depicted in Figure 4). The local dye concentrations of the samples used for the measurement were 0.30 mol/L for Rdots and 0.15 mol/L with 2 equiv of cyanostars to dyes for MERdots. These conditions were chosen since they represent the highest recorded Raman signal intensity for conventional Rdots (as shown in Figure S4) and MERdots (as shown in Figure 3b). Figure 4 highlights that the Raman signal intensity of MERdots

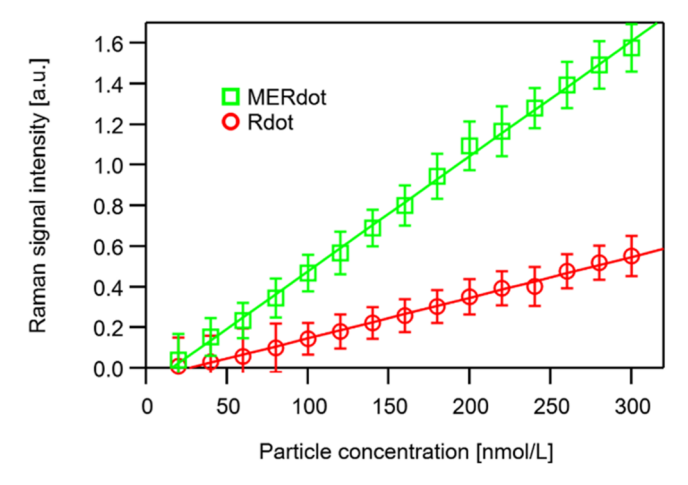


**Figure 4.** Concentration-dependent Raman signal intensity of conventional Rdots (red circles) and MERdots (green squares) in FT-CARS spectroscopy. The local concentrations of the samples used for the measurement were 0.30 mol/L for Rdots and 0.15 mol/L with 2 equiv of cyanostars to dyes for MERdots. The error bars indicate the standard deviations of the measured FT-CARS peak intensities (240 spectra).

is approximately 2.9 times higher than conventional Rdots (at a 300 nmol/L particle concentration). We also tested several other cyanine variants with 2 equiv of cyanostars to dyes, which display a similar increase of Raman signal intensity, and the Raman spectra are displayed in Figure S5. Also, the Raman cross section of MERdots is approximately 330 times higher than resonant dye molecules in solution and  $1.3 \times 10^8$  times higher than nonresonant Raman-active molecules such as methanol.<sup>33</sup> Furthermore, the particle concentration of MERdots at the detection limit is 69.0 nmol/L, which is a factor of 2.5 improvement over conventional Rdots with a limit of 170.6 nmol/L (as shown in Figure S6). The particle concentration of MERdots at the detection limit is also improved by a factor of  $4.3 \times 10^2$  compared to that of the dye molecules in solution with a limit of 29.4  $\mu$ mol/L (as shown in Figure S7).

This increase in Raman cross section is important for biological applications such as cell phenotyping or cancer detection by immunostaining. If we assume a lymphocyte with a diameter of  $\sim 10 \ \mu m$  as a sample, then by multiplying its volume by the detection limit concentrations of the brightest Rdots and MERdots, we can estimate that a minimum of  $5.4 \times$  $10^4$  Rdots/cell and  $2.1 \times 10^4$  MERdots/cell would be necessary for probe detection using our FT-CARS system. Immunostaining with Rdots has already been demonstrated<sup>22,23</sup> by attaching Rdots with antibodies and the same strategy is applicable to MERdots. Various studies have measured these values for different clusters of differentiation (CD) markers. According to a previous study on CD marker quantification<sup>36</sup> and under the assumption that all of the Rdot/ MERdot-labeled antibodies bind completely to the target antigens, only CD3, CD8, CD16, CD20, CD37, CD44, and CD45 could be detected using Rdots. This limit closely aligns with current fluorescence spectroscopic methods and does not showcase the full potential of Raman probes in super-multiplex biological imaging or flow cytometry. On the other hand, in addition to the previously mentioned 7 CD markers, CD2, CD4, CD5, CD7, CD11a, CD18, CD19, and CD24 could be detected by using MERdots, effectively doubling the number of

usable colors to 15. These additional CD markers possess unique qualities, which make them highly desirable for certain applications. For example, CD4 is commonly used in the diagnosis of HIV, <sup>37</sup> whereas CD19 has been used to diagnose cancers arising from B-cells. <sup>38</sup>

#### CONCLUSIONS

In conclusion, this study demonstrated the synthesis and characterization of novel nanoparticles, called macrocycleenhanced Rdots (MERdots), which incorporate both dye molecules and cyanostar macrocycles. The use of cyanostars allowed the dye molecules to be densely packed within the nanoparticle while circumventing dye aggregation by establishing interdye spacing, as inferred by the suppressed peak broadening observed in UV-vis absorption measurements. These characteristics of MERdots make them advantageous for achieving better and more predictable resonance Raman enhancement compared to conventional Rdots. We compared the Raman signal intensity of MERdots and conventional Rdots using an FT-CARS spectrometer and found that the signal intensity of MERdots with a local dye concentration of 0.10 mol/L increased as the amount of cyanostars was increased, while the amount of dye in the particle was kept constant. MERdots containing 3 molar equiv of cyanostar macrocycles relative to the dyes had the highest Raman signal intensity, which was 3.8 times higher than Rdots with the same local dye concentration without cyanostar incorporation. The optimal dye concentrations per nanoparticle for Rdots and MERdots containing 2 equiv of cyanostars to dyes were found, and when compared under the same particle concentration, the MERdots showed a 2.9-fold increase of the Raman signal intensity. Moreover, the detection limit on the concentration of MERdots was found to be improved by a factor of 2.5 compared to that of Rdots and a factor of 430 compared to that of Raman dye molecules in solution.

The results presented in this work suggest that MERdots have the potential to expand the application range of Raman tags in biomedical research due to their high brightness. For example, in the context of immunostaining, this increase in brightness would expand the variety of detectable CD markers. Toward future super-multiplex imaging or flow cytometry applications, various MERdots could be synthesized by incorporating various cyanine dyes, as displayed in Figure S5. Since these dyes are expected to have chemical properties similar to the IR740-Cl dye used in this study, multicolor MERdots can be produced using the same procedure outlined in this paper. This capability leverages the plug-and-play nature of the cyanostar-driven and hierarchical self-assembly of the SMILES materials that underpin the deaggregation of dyes present in the MERdots. However, it is important to consider the shift in absorption spectra that may occur upon the incorporation of different dyes into the MERdots, although the shift would not be that large and would have similar trends. Overall, this study provides a promising platform for the development of novel Raman probes with increased sensitivity and multiplexing capabilities.

## ASSOCIATED CONTENT

## Supporting Information

The Supporting Information is available free of charge at https://pubs.acs.org/doi/10.1021/acs.analchem.3c01958.

Fourier transform coherent anti-Stokes Raman scattering (FT-CARS) spectrometer schematic; absorption measurements for MERdots with various dye-macrocycle equivalents; SEM image of MERdots with 3 equiv of cyanostars to dyes and a local dye concentration of 0.125 mol/L; saturation of signal intensity in Rdots with increased local dye concentrations; increase of the Raman signal intensity of different variant IR740 Rdots by macrocycles in FT-CARS spectroscopy; representation of the mean minus three standard deviations as a function of particle concentration of conventional Rdots (red circles) and MERdots (green squares); concentration-dependent Raman signal intensity of the dye solution in FT-CARS spectroscopy (Figures S1–S7); amount of 60 mmol/L dye solution required for each Rdot; and amount of 30 mmol/L dye solution required for each MERdot (Tables S1 and S2) (PDF)

#### AUTHOR INFORMATION

### **Corresponding Authors**

Kotaro Hiramatsu — Department of Chemistry, The University of Tokyo, Tokyo 113-0033, Japan; Research Center for Spectrochemistry, The University of Tokyo, Tokyo 113-0033, Japan; ◎ orcid.org/0000-0003-0767-019X; Email: hiramatsu@chem.s.u-tokyo.ac.jp

Keisuke Goda — Department of Chemistry, The University of Tokyo, Tokyo 113-0033, Japan; Department of Bioengineering, University of California, Los Angeles, California 90095, United States; Institute of Technological Sciences, Wuhan University, Wuhan, Hubei 430072, P. R. China; orcid.org/0000-0001-6302-6038; Email: goda@chem.s.u-tokyo.ac.jp

#### **Authors**

Ryo Nishiyama – Department of Chemistry, The University of Tokyo, Tokyo 113-0033, Japan

Kei Furuya – Department of Chemistry, The University of Tokyo, Tokyo 113-0033, Japan

Phillip McCann – Department of Chemistry, The University of Tokyo, Tokyo 113-0033, Japan

Laura Kacenauskaite — Department of Chemistry, The University of Tokyo, Tokyo 113-0033, Japan; Present Address: Department of Chemistry, Stanford University, Stanford, CA 94305-5080 United States

Bo W. Laursen – Nano-Science Center and Department of Chemistry, University of Copenhagen, DK-2100 Copenhagen, Denmark

Amar H. Flood — Department of Chemistry, Indiana University Bloomington, Bloomington, Indiana 47405, United States; © orcid.org/0000-0002-2764-9155

Complete contact information is available at: https://pubs.acs.org/10.1021/acs.analchem.3c01958

#### **Author Contributions**

VR.N., K.F., and P.M. contributed equally to this work. The manuscript was written through contributions of all authors. All authors have given approval to the final version of the manuscript.

## Notes

The authors declare the following competing financial interest(s): K.G. is a shareholder of CYBO and LucasLand. R.N., K.F., P.M., L.K., B.W.L., A.F., K.H., and K.G. are filing a

patent for MERDots. B.W.L. and A.F. are cofounders of Halophore, Inc. and have filed a patent on SMILES technology.

## ACKNOWLEDGMENTS

This work was supported by JST PRESTO (JPMJPR1878), JST FOREST (21470594), JSPS Gran-in-Aid for Scientific Research (B) (22538379), JSPS Grant-in-Aid for Young Scientists (20K15227), JSPS Core-to-Core Program, Research Foundation for Opto-Science and Technology, and Advanced Research Infrastructure for Materials and Nanotechnology in Japan (ARIM) of the Ministry of Education, Culture, Sports, Science and Technology (MEXT) (JPMXP1222UT0376). A.H.F. acknowledges support from the US National Science Foundation (DMR-2118423).

#### REFERENCES

- (1) Huang, B.; Bates, M.; Zhuang, X. Annu. Rev. Biochem. 2009, 78, 993-1016.
- (2) Bünzli, J.-C. G. Chem. Rev. 2010, 110, 2729-2755.
- (3) Vaneycken, I.; D'huyvetter, M.; Hernot, S.; de Vos, J.; Xavier, C.; Devoogdt, N.; Caveliers, V.; Lahoutte, T. *Curr. Opin. Biotechnol.* **2011**, 22, 877–881.
- (4) Adan, A.; Alizada, G.; Kiraz, Y.; Baran, Y.; Nalbant, A. Crit. Rev. Biotechnol. 2017, 37, 163–176.
- (5) Cossarizza, A.; Chang, H. D.; Radbruch, A.; Acs, A.; Adam, D.; Adam-Klages, S.; Agace, W. W.; Aghaeepour, N.; Akdis, M.; Allez, M.; Almeida, L. N.; Alvisi, G.; Anderson, G.; Andrä, I.; Annunziato, F.; Anselmo, A.; Bacher, P.; Baldari, C. T.; Bari, S.; Barnaba, V.; Barros-Martins, J.; Battistini, L.; Bauer, W.; Baumgart, S.; Baumgarth, N.; Baumjohann, D.; Baying, B.; Bebawy, M.; Becher, B.; Beisker, W.; Benes, V.; Beyaert, R.; Blanco, A.; Boardman, D. A.; Bogdan, C.; Borger, J. G.; Borsellino, G.; Boulais, P. E.; Bradford, J. A.; Brenner, D.; Brinkman, R. R.; Brooks, A. E. S.; Busch, D. H.; Büscher, M.; Bushnell, T. P.; Calzetti, F.; Cameron, G.; Cammarata, I.; Cao, X.; Cardell, S. L.; Casola, S.; Cassatella, M. A.; Cavani, A.; Celada, A.; Chatenoud, L.; Chattopadhyay, P. K.; Chow, S.; Christakou, E.; Čičin-Šain, L.; Clerici, M.; Colombo, F. S.; Cook, L.; Cooke, A.; Cooper, A. M.; Corbett, A. J.; Cosma, A.; Cosmi, L.; Coulie, P. G.; Cumano, A.; Cvetkovic, L.; Dang, V. D.; Dang-Heine, C.; Davey, M. S.; Davies, D.; De Biasi, S.; Zotto, G. D.; Cruz, G. V. D.; Delacher, M.; Della Bella, S.; Dellabona, P.; Deniz, G.; Dessing, M.; Di Santo, J. P.; Diefenbach, A.; Dieli, F.; Dolf, A.; Dörner, T.; Dress, R. J.; Dudziak, D.; Dustin, M.; Dutertre, C. A.; Ebner, F.; Eckle, S. B. G.; Edinger, M.; Eede, P.; Ehrhardt, G. R. A.; Eich, M.; Engel, P.; Engelhardt, B.; Erdei, A.; Esser, C.; Everts, B.; Evrard, M.; Falk, C. S.; Fehniger, T. A.; Felipo-Benavent, M.; Ferry, H.; Feuerer, M.; Filby, A.; Filkor, K.; Fillatreau, S.; Follo, M.; Förster, I.; Foster, J.; Foulds, G. A.; Frehse, B.; Frenette, P. S.; Frischbutter, S.; Fritzsche, W.; Galbraith, D. W.; Gangaev, A.; Garbi, N.; Gaudilliere, B.; Gazzinelli, R. T.; Geginat, J.; Gerner, W.; Gherardin, N. A.; Ghoreschi, K.; Gibellini, L.; Ginhoux, F.; Goda, K.; Godfrey, D. I.; Goettlinger, C.; González-Navajas, J. M.; Goodyear, C. S.; Gori, A.; Grogan, J. L.; Grummitt, D.; Grützkau, A.; Haftmann, C.; Hahn, J.; Hammad, H.; Hämmerling, G.; Hansmann, L.; Hansson, G.; Harpur, C. M.; Hartmann, S.; Hauser, A.; Hauser, A. E.; Haviland, D. L.; Hedley, D.; Hernández, D. C.; Herrera, G.; Herrmann, M.; Hess, C.; Höfer, T.; Hoffmann, P.; Hogquist, K.; Holland, T.; Höllt, T.; Holmdahl, R.; Hombrink, P.; Houston, J. P.; Hoyer, B. F.; Huang, B.; Huang, F. P.; Huber, J. E.; Huehn, J.; Hundemer, M.; Hunter, C. A.; Hwang, W. Y. K.; Iannone, A.; Ingelfinger, F.; Ivison, S. M.; Jäck, H. M.; Jani, P. K.; Jávega, B.; Jonjic, S.; Kaiser, T.; Kalina, T.; Kamradt, T.; Kaufmann, S. H. E.; Keller, B.; Ketelaars, S. L. C.; Khalilnezhad, A.; Khan, S.; Kisielow, J.; Klenerman, P.; Knopf, J.; Koay, H. F.; Kobow, K.; Kolls, J. K.; Kong, W. T.; Kopf, M.; Korn, T.; Kriegsmann, K.; Kristyanto, H.; Kroneis, T.; Krueger, A.; Kühne, J.; Kukat, C.; Kunkel, D.; Kunze-Schumacher, H.; Kurosaki, T.; Kurts, C.; Kvistborg, P.; Kwok, I.;

Landry, J.; Lantz, O.; Lanuti, P.; LaRosa, F.; Lehuen, A.; LeibundGut-Landmann, S.; Leipold, M. D.; Leung, L. Y. T.; Levings, M. K.; Lino, A. C.; Liotta, F.; Litwin, V.; Liu, Y.; Ljunggren, H. G.; Lohoff, M.; Lombardi, G.; Lopez, L.; López-Botet, M.; Lovett-Racke, A. E.; Lubberts, E.; Luche, H.; Ludewig, B.; Lugli, E.; Lunemann, S.; Maecker, H. T.; Maggi, L.; Maguire, O.; Mair, F.; Mair, K. H.; Mantovani, A.; Manz, R. A.; Marshall, A. J.; Martínez-Romero, A.; Martrus, G.; Marventano, I.; Maslinski, W.; Matarese, G.; Mattioli, A. V.; Maueröder, C.; Mazzoni, A.; McCluskey, J.; McGrath, M.; McGuire, H. M.; McInnes, I. B.; Mei, H. E.; Melchers, F.; Melzer, S.; Mielenz, D.; Miller, S. D.; Mills, K. H. G.; Minderman, H.; Mjösberg, J.; Moore, J.; Moran, B.; Moretta, L.; Mosmann, T. R.; Müller, S.; Multhoff, G.; Muñoz, L. E.; Münz, C.; Nakayama, T.; Nasi, M.; Neumann, K.; Ng, L. G.; Niedobitek, A.; Nourshargh, S.; Núñez, G.; O'Connor, J. E.; Ochel, A.; Oja, A.; Ordonez, D.; Orfao, A.; Orlowski-Oliver, E.; Ouyang, W.; Oxenius, A.; Palankar, R.; Panse, I.; Pattanapanyasat, K.; Paulsen, M.; Pavlinic, D.; Penter, L.; Peterson, P.; Peth, C.; Petriz, J.; Piancone, F.; Pickl, W. F.; Piconese, S.; Pinti, M.; Pockley, A. G.; Podolska, M. J.; Poon, Z.; Pracht, K.; Prinz, I.; Pucillo, C. E. M.; Quataert, S. A.; Quatrini, L.; Quinn, K. M.; Radbruch, H.; Radstake, T. R. D. J.; Rahmig, S.; Rahn, H. P.; Rajwa, B.; Ravichandran, G.; Raz, Y.; Rebhahn, J. A.; Recktenwald, D.; Reimer, D.; Reis e Sousa, C.; Remmerswaal, E. B. M.; Richter, L.; Rico, L. G.; Riddell, A.; Rieger, A. M.; Robinson, J. P.; Romagnani, C.; Rubartelli, A.; Ruland, J.; Saalmüller, A.; Saeys, Y.; Saito, T.; Sakaguchi, S.; Sala-de-Oyanguren, F.; Samstag, Y.; Sanderson, S.; Sandrock, I.; Santoni, A.; Sanz, R. B.; Saresella, M.; Sautes-Fridman, C.; Sawitzki, B.; Schadt, L.; Scheffold, A.; Scherer, H. U.; Schiemann, M.; Schildberg, F. A.; Schimisky, E.; Schlitzer, A.; Schlosser, J.; Schmid, S.; Schmitt, S.; Schober, K.; Schraivogel, D.; Schuh, W.; Schüler, T.; Schulte, R.; Schulz, A. R.; Schulz, S. R.; Scottá, C.; Scott-Algara, D.; Sester, D. P.; Shankey, T. V.; Silva-Santos, B.; Simon, A. K.; Sitnik, K. M.; Sozzani, S.; Speiser, D. E.; Spidlen, J.; Stahlberg, A.; Stall, A. M.; Stanley, N.; Stark, R.; Stehle, C.; Steinmetz, T.; Stockinger, H.; Takahama, Y.; Takeda, K.; Tan, L.; Tárnok, A.; Tiegs, G.; Toldi, G.; Tornack, J.; Traggiai, E.; Trebak, M.; Tree, T. I. M.; Trotter, J.; Trowsdale, J.; Tsoumakidou, M.; Ulrich, H.; Urbanczyk, S.; van de Veen, W.; van den Broek, M.; van der Pol, E.; Van Gassen, S.; Van Isterdael, G.; van Lier, R. A. W.; Veldhoen, M.; Vento-Asturias, S.; Vieira, P.; Voehringer, D.; Volk, H. D.; von Borstel, A.; von Volkmann, K.; Waisman, A.; Walker, R. V.; Wallace, P. K.; Wang, S. A.; Wang, X. M.; Ward, M. D.; Ward-Hartstonge, K. A.; Warnatz, K.; Warnes, G.; Warth, S.; Waskow, C.; Watson, J. V.; Watzl, C.; Wegener, L.; Weisenburger, T.; Wiedemann, A.; Wienands, J.; Wilharm, A.; Wilkinson, R. J.; Willimsky, G.; Wing, J. B.; Winkelmann, R.; Winkler, T. H.; Wirz, O. F.; Wong, A.; Wurst, P.; Yang, J. H. M.; Yang, J.; Yazdanbakhsh, M.; Yu, L.; Yue, A.; Zhang, H.; Zhao, Y.; Ziegler, S. M.; Zielinski, C.; Zimmermann, J.; Zychlinsky, A. Eur. J. Immunol. 2019, 49, 1457-1973.

- (6) Mikami, H.; Kawaguchi, M.; Huang, C. J.; Matsumura, H.; Sugimura, T.; Huang, K.; Lei, C.; Ueno, S.; Miura, T.; Ito, T.; Nagasawa, K.; Maeno, T.; Watarai, H.; Yamagishi, M.; Uemura, S.; Ohnuki, S.; Ohya, Y.; Kurokawa, H.; Matsusaka, S.; Sun, C. W.; Ozeki, Y.; Goda, K. *Nat. Commun.* **2020**, *11*, No. 1162.
- (7) Nitta, N.; Sugimura, T.; Isozaki, A.; Mikami, H.; Hiraki, K.; Sakuma, S.; Iino, T.; Arai, F.; Endo, T.; Fujiwaki, Y.; Fukuzawa, H.; Hase, M.; Hayakawa, T.; Hiramatsu, K.; Hoshino, Y.; Inaba, M.; Ito, T.; Karakawa, H.; Kasai, Y.; Koizumi, K.; Lee, S. W.; Lei, C.; Li, M.; Maeno, T.; Matsusaka, S.; Murakami, D.; Nakagawa, A.; Oguchi, Y.; Oikawa, M.; Ota, T.; Shiba, K.; Shintaku, H.; Shirasaki, Y.; Suga, K.; Suzuki, Y.; Suzuki, N.; Tanaka, Y.; Tezuka, H.; Toyokawa, C.; Yalikun, Y.; Yamada, M.; Yamagishi, M.; Yamano, T.; Yasumoto, A.; Yatomi, Y.; Yazawa, M.; Di Carlo, D.; Hosokawa, Y.; Uemura, S.; Ozeki, Y.; Goda, K. Cell 2018, 175, 266–276.
- (8) Perfetto, S. P.; Chattopadhyay, P. K.; Roederer, M. Nat. Rev. Immunol. 2004, 4, 648-655.
- (9) Zhang, J.; Campbell, R. E.; Ting, A. Y.; Tsien, R. Y. Nat. Rev. Mol. Cell Biol. 2002, 3, 906–918.

- (10) Miao, Y.; Shi, L.; Hu, F.; Min, W. Phys. Biol. 2019, 16, No. 041003.
- (11) Zavaleta, C. L.; Smith, B. R.; Walton, I.; Doering, W.; Davis, G.; Shojaei, B.; Natan, M. J.; Gambhir, S. S. *Proc. Natl. Acad. Sci. U.S.A.* **2009**, *106*, 13511–13516.
- (12) Yamakoshi, H.; Dodo, K.; Okada, M.; Ando, J.; Palonpon, A.; Fujita, K.; Kawata, S.; Sodeoka, M. *J. Am. Chem. Soc.* **2011**, *133*, 6102–6105.
- (13) Li, Y.; Wang, Z.; Mu, X.; Ma, A.; Guo, S. Biotechnol. Adv. 2017, 35, 168-177.
- (14) Liu, L.; Pancorbo, P. M.; Xiao, T. H.; Noguchi, S.; Marumi, M.; Segawa, H.; Karhadkar, S.; de Pablo, J. G.; Hiramatsu, K.; Kitahama, Y.; Itoh, T.; Qu, J.; Takei, K.; Goda, K. *Adv. Opt. Mater.* **2022**, *10*, No. 2200054.
- (15) Itoh, T.; Procházka, M.; Dong, Z.-C.; Ji, W.; Yamamoto, Y. S.; Zhang, Y.; Ozaki, Y. Chem. Rev. 2023, 123, 1552–1634.
- (16) Laing, S.; Jamieson, L. E.; Faulds, K.; Graham, D. Nat. Rev. Chem. 2017, 1, No. 0060.
- (17) Chen, N.; Xiao, T. H.; Luo, Z.; Kitahama, Y.; Hiramatsu, K.; Kishimoto, N.; Itoh, T.; Cheng, Z.; Goda, K. *Nat. Commun.* **2020**, *11*, No. 4772
- (18) Wang, Y.; Yan, B.; Chen, L. Chem. Rev. 2013, 113, 1391-1428.
- (19) Tian, S.; Li, H.; Li, Z.; Tang, H.; Yin, M.; Chen, Y.; Wang, S.; Gao, Y.; Yang, X.; Meng, F.; Lauher, J. W.; Wang, P.; Luo, L. *Nat. Commun.* **2020**, *11*, No. 81.
- (20) Yamakoshi, H.; Dodo, K.; Palonpon, A.; Ando, J.; Fujita, K.; Kawata, S.; Sodeoka, M. J. Am. Chem. Soc. 2012, 134, 20681–20689.
- (21) Matanfack, G. A.; Rüger, J.; Stiebing, C.; Schmitt, M.; Popp, J. J. Biophotonics **2020**, 13, No. e202000129.
- (22) Zhao, Z.; Chen, C.; Wei, S.; Xiong, H.; Hu, F.; Miao, Y.; Jin, T.; Min, W. Nat. Commun. 2021, 12, No. 1305.
- (23) Chen, C.; Zhao, Z.; Qian, N.; Wei, S.; Hu, F.; Min, W. Nat. Commun. 2021, 12, No. 3405.
- (24) Caram, J. R.; Deshmukh, A. P.; Bailey, A. D.; Forte, L. S.; Shen, X.; Geue, N.; Sletten, E. M. J. Phys. Chem. Lett. **2020**, *11*, 8026–8033.
- (25) Deshmukh, A. P.; Koppel, D.; Chuang, C.; Cadena, D. M.; Cao, J.; Caram, J. R. J. Phys. Chem. C 2019, 123, 18702–18710.
- (26) Lee, S.; Chen, C. H.; Flood, A. H. Nat. Chem. 2013, 5, 704-710.
- (27) Chen, J.; Fateminia, S. M. A.; Kacenauskaite, L.; Bærentsen, N.; Stenspil, S. G.; Bredehoeft, J.; Martinez, K. L.; Flood, A. H.; Laursen, B. W. Angew. Chem., Int. Ed. 2021, 60, 9450–9458.
- (28) Kacenauskaite, L.; Stenspil, S. G.; Olsson, A. H.; Flood, A. H.; Laursen, B. W. J. Am. Chem. Soc. 2022, 144, 19981–19989.
- (29) Chen, J.; Stenspil, S. G.; Kaziannis, S.; Kacenauskaite, L.; Lenngren, N.; Kloz, M.; Flood, A. H.; Laursen, B. W. ACS Appl. Nano Mater. 2022, 5, 13887–13893.
- (30) Benson, C. R.; Kacenauskaite, L.; Vandenburgh, K. L.; Raghavachari, K.; Laursen, B. W.; Flood, A. H.; Zhao, W.; Qiao, B.; Sadhukhan, T.; Pink, M.; Chen, J.; Borgi, S.; Chen, C.-H.; Davis, B. J.; Simon, Y. C. *Chem* **2020**, *6*, 1978–1997.
- (31) Qiao, B.; Hirsch, B. E.; Lee, S.; Pink, M.; Chen, C. H.; Laursen, B. W.; Flood, A. H. *J. Am. Chem. Soc.* **2017**, *139*, 6226–6233.
- (32) Haketa, Y.; Sasaki, S.; Ohta, N.; Masunaga, H.; Ogawa, H.; Mizuno, N.; Araoka, F.; Takezoe, H.; Maeda, H. *Angew. Chem., Int. Ed.* **2010**, 49, 10079–10083.
- (33) Nishiyama, R.; Hiramatsu, K.; Kawamura, S.; Dodo, K.; Furuya, K.; de Pablo, J. G.; Takizawa, S.; Min, W.; Sodeoka, M.; Goda, K. *PNAS Nexus* **2023**, *2*, No. pgad001.
- (34) Zhao, Z.; Chen, C.; Wei, S.; Xiong, H.; Hu, F.; Miao, Y.; Jin, T.; Min, W. Nat. Commun. 2021, 12, No. 1305.
- (35) Chen, J.; Stenspil, S. G.; Kaziannis, S.; Kacenauskaite, L.; Lenngren, N.; Kloz, M.; Flood, A. H.; Laursen, B. W. ACS Appl. Nano Mater. 2022, 5, 13887–13893.
- (36) Bikoue, A.; George, F.; Poncelet, P.; Mutin, M.; Janossy, G.; Sampol, J. Cytometry 1996, 26, 137–147.
- (37) Filion, L. G.; Izaguirre, C. A.; Garber, G. E.; Huebsh, L.; Aye, M. T. J. Immunol. Methods 1990, 135, 59–69.

(38) Scheuermann, R. H.; Racila, E. Leuk. Lymphoma 1995, 18, 385-397.